

Modeling Effective Stiffness Properties of IAD Fabrics

Scott M. Murman

Scott.M.Murman@nasa.gov

NASA Ames Research Center, Moffett Field, CA, USA

Srinivasan A. Suresh*

ssuresh@princeton.edu

Princeton University, Princeton, NJ, USA

Abstract

A model for the mechanical stiffness properties of bladder fabrics for inflatable decelerators under high stress conditions is developed. This planar orthotropic model uses understanding of the fabric behavior, analytical modeling, numerical simulations, and available experimental data to characterize the fabric stiffness (elastic modulus), contraction (Poisson's ratio), and shear modulus. The derived model is designed to integrate with standard finite-element methods and is validated against available static test data for two types of silicone-coated Kevlar fabric using the commercial LS-DYNA solver.

1 Introduction

NASA is investigating inflatable aerodynamic decelerator (IAD) concepts to improve the delivery of high-mass missions to the surface of Mars[1, 2]. IADs typically deploy pressurized sections constructed from lightweight impermeable fabrics to decrease the ballistic coefficient of the entry vehicle during descent (cf. Fig. 1). These concepts also have the potential to control the aerodynamic response, *e.g.*, by forcing the bluff-body separation location using a “burble fence.” High-fidelity analysis of these concepts requires prediction of the fabric response in a complex aerodynamic environment. Detailed predictions of the fabric stiffness, damping, and potential for wrinkling (buckling) under dynamic and thermal loading are required. This data is difficult to obtain from sub-scale or ground testing, and it is anticipated that validated numerical methods will fill this role.

*2010 Summer Intern, Mission Critical Technologies, Inc., Sunnyvale, CA.

This material is declared a work of the U.S. Government and is not subject to copyright protection in the United States.

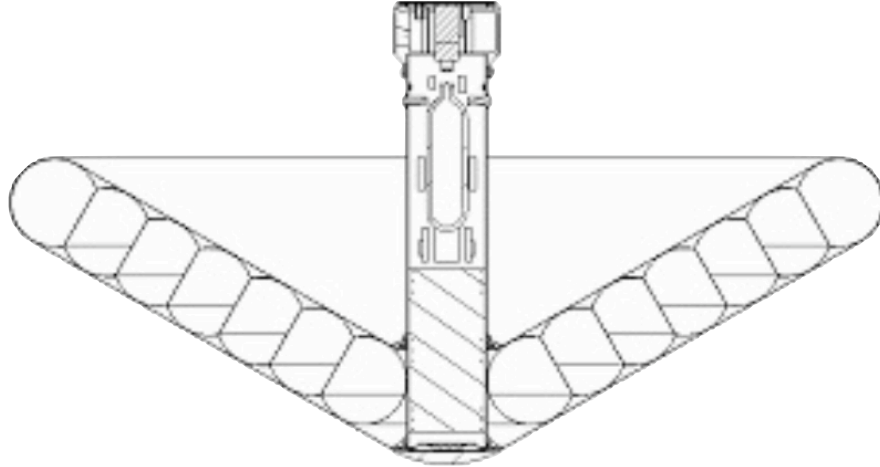


Figure 1: Stacked toroid inflatable aerodynamic decelerator concept. Pressurized toroids of gas are surrounded by a composite of impermeable bladder and thermal protection systems fabrics.

A fabric is a structure, comprised of fibres twisted to form yarns, with these yarns woven together to form the fabric itself. Prospective IAD bladder materials add an impermeable coating, such as silicone or urethane, to the structure. Direct structural analysis of the fabric is possible using micromechanical modeling of the yarn properties, friction of the weave, *etc.* [3, 4]. Micromechanical simulations provide controlled numerical experiments to extract detailed information regarding the fabric structural response. Unfortunately, these techniques are computationally intensive, and not currently practical for application to a full-scale flight vehicle. Mesomechanical methods, which model many of the micromechanical features on an intermediate scale are also possible [5, 6], however these require developing specialized algorithms and corresponding validation. In lieu of these higher-fidelity methods, we approximate the fabric as a homogeneous material, and seek models of the “effective” mechanical behavior for use in traditional finite-element models (FEM). This approach leverages the existing infrastructure of FEM codes, reducing development and simulation costs, while still providing sufficient accuracy for the majority of engineering problems of interest for inflatable decelerators.

Fabrics are important engineering structures in many fields, and there have been several studies examining the response of fabric structures, coated or uncoated, under load [7–11]. Similarly, several studies have proposed modeling approaches targeted to specific applications, *e.g.* medical, manufacturing, architecture, *etc.* These models are either based on first principles [7, 12], empirical [13], or are combinations of the two approaches [11]. The primary objective here is to leverage this previous work in testing and modeling to develop an engineering model of coated woven fabrics special-

Denier	TPI	Uncoated Areal Density (oz/yd ²)	Coated Areal Density (oz/yd ²)	Uncoated Thickness (in)	Coated Thickness (in)
200	40	2.1	8.0	0.005	0.008
840	26	5.8	10.2	0.010	0.014

Table 1: Properties of two silicone-coated plain-weave Kevlar fabrics which are representative of the field of IAD bladder fabrics.

ized for inflatable decelerators. This emphasizes both the high tension these structures encounter, and also their large scale, with deployed dimensions being 10 ft. or greater in diameter. The approach combines understanding of the fabric behavior, analytical modeling, numerical simulations, and available experimental data[14, 15] to develop validated models of the effective stiffness appropriate for FEM and Fluid-Structure-Interaction (FSI) simulations. Bending and damping properties are left for future work.

2 Background

Several recent studies have characterized the mechanical properties of a variety of coated woven fabrics appropriate for IAD systems[14–16], providing a relatively broad database of experimental results from which trends can be extracted. In order to clarify the discussion, the current work focuses on two silicone-coated plain-weave Kevlar fabrics from [15], which are representative of the overall trends. The details of the Kevlar samples are provided in Table 1.

Fabrics display several response mechanisms that differ from traditional solid mechanics. These include: *friction* as the yarns slide across each other, *crimp interchange* (cf. Fig. 2) is the transfer of crimp (waviness of the yarn) from one fabric direction to another as a result of loading, *slip*, where the yarns rotate relative to each other in shear, and *locking*, where the interwoven yarns jam against each other. Understanding these different behaviors is important for interpreting experimental test results and developing an appropriate model for the fabric response.

All of the models examined in this work assume a planar orthotropic material. The stiffness matrix relating stress to strain in the principal coordinate system for a planar orthotropic material is given by

$$\begin{Bmatrix} \sigma_1 \\ \sigma_2 \\ \tau_{12} \end{Bmatrix} = \begin{bmatrix} \frac{E_1}{1-\nu_{12}\nu_{21}} & \frac{\nu_{12}E_2}{1-\nu_{12}\nu_{21}} & 0 \\ \frac{\nu_{21}E_1}{1-\nu_{12}\nu_{21}} & \frac{E_2}{1-\nu_{12}\nu_{21}} & 0 \\ 0 & 0 & G_{12} \end{bmatrix} \begin{Bmatrix} \epsilon_1 \\ \epsilon_2 \\ \gamma_{12} \end{Bmatrix} \quad (1)$$

where $\gamma_{12} = 2\epsilon_{12}$ is the engineering shear strain, E_i are the elastic moduli, G_{12} is the shear modu-

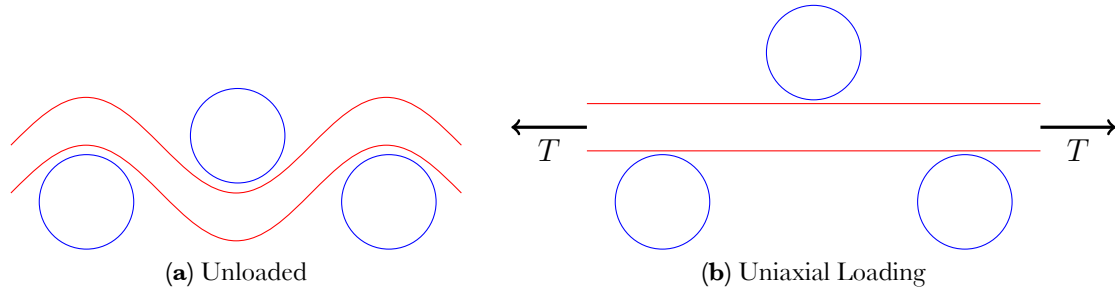


Figure 2: Idealized representation of crimp interchange. Loading along the yarns (red) straightens them (decreasing their crimp), while simultaneously forcing the crimp in the opposing direction (blue) to increase.

lus, and ν_{12} , ν_{21} are the orthotropic Poisson's ratio. By symmetry, $\nu_{21} = \nu_{12} \frac{E_2}{E_1}$. The out-of-plane response is considered decoupled from the in-plane response. For plain-weave fabrics we assume $E_1 = E_2$ and $\nu_{12} = \nu_{21}$. The focus of the current work is determining appropriate entries in the orthotropic stiffness matrix to represent the coated fabric response for typical atmospheric decelerator applications. It is assumed that the fabric has negligible resistance to compressive loading.

The commercial LS-DYNA FEM solver provides an attractive test-bed to evaluate the predictive capability of the proposed models for material properties. LS-DYNA is heavily used in several industries, and has been validated for complex fabric response, such as airbag deployment and bulletproof vests. Further, LS-DYNA provides the ability to experiment with different formulations, *e.g.*, membrane *vs.* thin-shell, along with “user-defined” material models which leverage the existing infrastructure of the FEM solver. Where appropriate in the discussion, details on the methods used with the LS-DYNA simulations are provided.

3 Fabric Modeling

There are several methods for developing models of fabric response, ranging from first principles to empirical observations. The approach taken here is to utilize knowledge of the fabric behavior and geometry to develop a modeling framework, and augment that framework with experimental observations, both physical and virtual.

3.1 Axial Loading

The primary effect to model is the stiffness of the fabric under loading aligned with the warp or weft directions, *i.e.* uniaxial loading. This determines the tensile strength of the fabric, and provides a base to build up more complex behavior such as lateral contraction, biaxial loading, *etc.* The

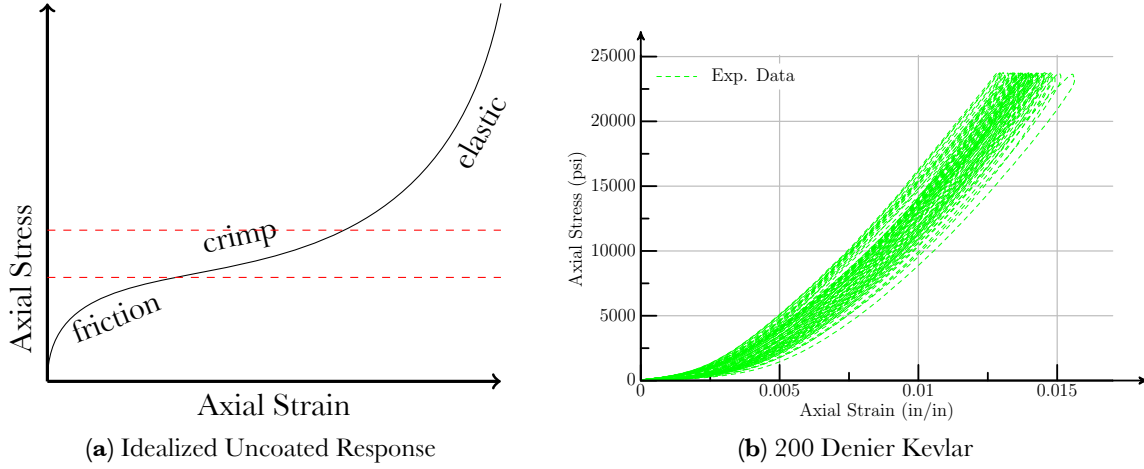


Figure 3: Uniaxial stress-strain variation for an idealized uncoated fabric and a coated woven fabric. The experimental response for the coated fabric begins immediately with crimp interchange. Experimental data taken from [15].

idealized response of a fabric under tension is presented in Fig. 3a (cf. Cavallaro *et al.*[8]). Initially the yarns slide with resistance due to friction. As the load increases crimp interchange occurs, ultimately giving way to an elastic behavior. Fig. 3b presents representative load cycles of the coated 200 denier Kevlar fabric in a uniaxial test rig[15]. As expected, the coated fabric immediately begins crimp interchange when loaded, as the coating inhibits movement between the yarns. Subsequent to this crimp interchange the fabric demonstrates a predominately linearly-elastic response with the slope representing the elastic modulus E_1 in Eqn. 1.

As a proof of concept, the response to uniaxial loading is modeled using a bilinear elastic modulus in the LS-DYNA MAT_FABRIC material model,

$$E_1 = \begin{cases} E_1^c & \text{if } \epsilon_1 \leq \epsilon^c, \\ E_1^o & \text{if } \epsilon_1 > \epsilon^c. \end{cases} \quad (2)$$

For the 200 denier Kevlar fabric, $E_1^o = 2.2 \times 10^6$ psi, $E_1^c = 0.1 E_1^o$, and $\epsilon^c = 0.00375$ in/in. The bilinear model accurately reproduces the median response of test specimen, including the crimp interchange (cf. Fig. 4). The bilinear model predictions demonstrate that it is possi-

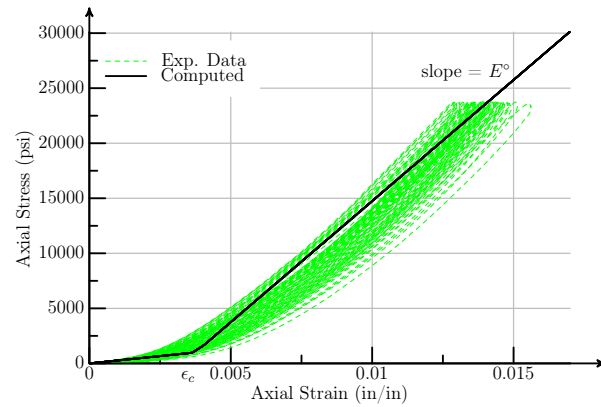


Figure 4: Uniaxial stress-strain variation for silicone-coated Kevlar fabrics modeled using a bilinear elastic modulus. Experimental data taken from [15].

ble to replicate the nonlinear crimp interchange, however doing so in a predictive sense, for different weave patterns, thread densities, *etc.* is difficult. Both the strain and the elastic modulus which define the crimp interchange region must be determined empirically.* Seebring and Freeston[17, 18] model the crimp interchange, including the crimp interchange strain, however the model predictions are inconsistent across the database of coated fabric samples tested to-date. Other researchers have suggested that mesomechanical information, lacking in a homogeneous FEM model, is required for predicting the crimp interchange[6, 12].

A further complication is the pathology of uniaxial loading. Under pure biaxial loading the crimp interchange is not present (cf. [17, 18]), only appearing when the loading in one yarn direction dominates. To account for this, the nonlinearity in the crimp interchange region is selectively enabled when uniaxial loading is detected via a sensor function,

$$\beta(\sigma_1, \sigma_2) = \min \left(1, \frac{(\sigma_1 - \sigma_2)^2}{(\sigma_1 + \sigma_2)^2} \right) \quad (3)$$

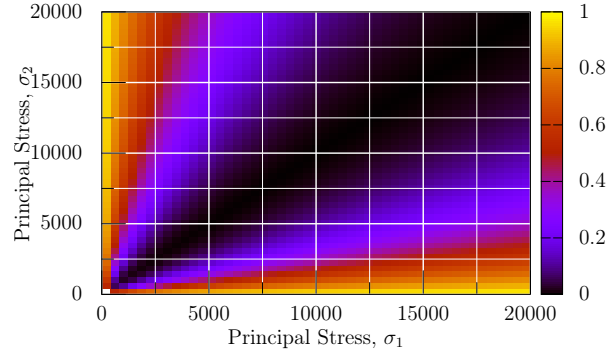


Figure 5: Biaxial sensor function, Eqn. 3.

This sensor is unity for uniaxial loading, and rapidly approaches zero under biaxial stress (cf. Fig. 5). The sensor provides an automatic switching for the elastic modulus,

$$E_i = \begin{cases} E_i^o - \beta(\sigma_1, \sigma_2)(E_i^o - E_i^c) & \text{if } \epsilon_i \leq \epsilon_i^c, \\ E_i^o & \text{if } \epsilon_i > \epsilon_i^c. \end{cases} \quad (4)$$

This reproduces the qualitative behavior observed in published biaxial loading responses (cf. [10, 11, 13]), however general biaxial test data is not currently available to validate the approach for coated IAD fabrics. Note that many IAD designs contain purely biaxially loaded structures, such as inflated toroids and pre-tensioned gore panels (cf. Fig. 1). In these cases it is possible to *a priori* simplify the modeling approach to neglect the nonlinear crimp interchange region.

3.2 Approximate Elastic Modulus

The elastic modulus is normally estimated from uniaxial test data using empirical modeling, for example a linear regression to determine the nominal slope of the stress-strain response. One alter-

*A method to predict the elastic modulus in the linear elastic is presented in the next section.

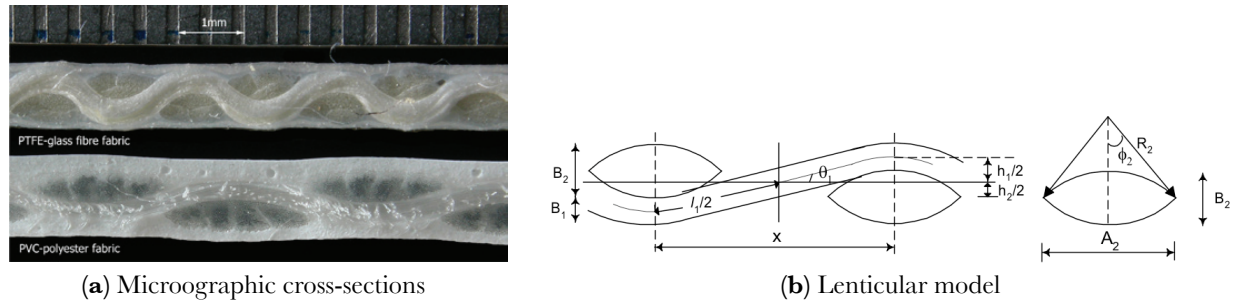


Figure 6: Lenticular fabric cross-section model for compressed weave from [19]. Micrograph cross-sections of PTFE-glass and PVS-polyester fabrics courtesy Prof. Peter Gosling and Dr. Ben Bridgens, Newcastle University, UK.

Denier	Measured (psi)	Modeled (psi)
200	2.20×10^6	2.25×10^6
840	3.50×10^6	3.54×10^6

Table 2: Elastic modulus E_1^o of the silicone-coated plain-weave Kevlar fabrics.

native is to develop a simple predictive model for the elastic response which is used in the absence of uniaxial test data, or as part of a design process. The assumption is that the axial loading is taken completely by the yarns in the loading direction, with stiffness of the applied coating being negligible. This convenience allows estimates of the axial stiffness purely from geometrical properties of the fabric and the strength of the fibres. Fibre data is relatively easy to obtain, while measured stiffness for the fabric structure itself requires dedicated testing which is not readily available.

The fabric yarns themselves are compressed (flattened) during weaving due to inter-yarn pressure (cf. Fig. 6a and Fig. 3 from [13]). Following Hearle and Shanahan[19], we adopt a lenticular cross-sectional shape for the yarns (cf. Fig. 6b). It is assumed that the height (b) of each lens is half the uncoated fabric thickness (t), and the width of each lens (a) is twice the height. From this, and the number of threads-per-inch (TPI) of the weave pattern, the load-bearing area of a fabric cross-section is estimated. The fibre elastic modulus is available through material data sheets (MDS). Table 2 presents the elastic modulus determined using the approximate model, and the value obtained from the elastic response region of the uniaxial test samples, for two weights of silicone-coated Kevlar fabric. The agreement between the simplified model and the regression of the experimental data in the linear-elastic regime is very good in both cases.

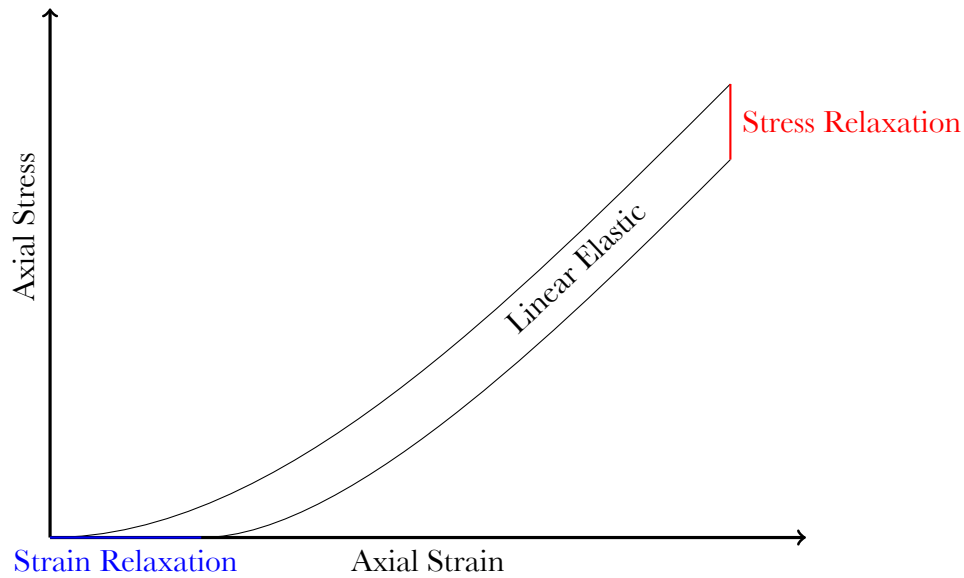


Figure 7: Idealized hysteresis of fabric response during uniaxial loading cycles.

3.3 Hysteresis

The experimental uniaxial loading cycles in Fig. 3 demonstrate appreciable hysteresis, and also “wander” between cycles. Commonly, hysteresis is modeled using a rate-dependent damping term. The experimental loading cycles use a low crosshead speed, and it is not possible to replicate the observed hysteresis using plausible values of damping coefficient. An idealized uniaxial loading hysteresis cycle is presented in Fig. 7. At the top of the load cycle the crosshead is held fixed for a short period. During this stasis the stress in the fabric “relaxes” without any change in strain or strain rate. Similarly, at the bottom of the cycle, the residual strain in the fabric relaxes without any change in stress. This relaxation process is responsible for the observed hysteresis. The timescale of the relaxation is greater than the pause at the peaks of the load and unload cycles, leading to the wandering of the stress-strain response curves.

It is difficult to directly model the relaxation hysteresis of the fabric response by modifying the stiffness or damping matrices of a typical FEM. During the load relaxation there is no increment in strain (or strain rate) present to alter the stress, and vice versa during the unload relaxation. It is possible to replicate the observed hysteresis using an inertial lag technique, which is also consistent with the physics of the fabric response. Unlike a solid specimen, where the load essentially is instantaneously transferred through the entire specimen, in a fabric the loading in different regions

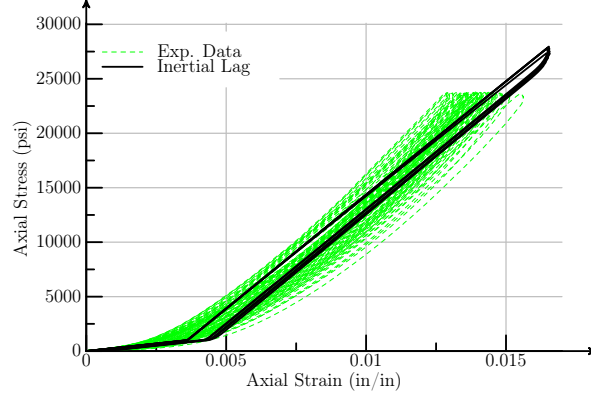


Figure 8: Simulations of hysteresis for 200 denier Kevlar in a uniaxial test rig using LS-DYNA with an inertial lag, $C_{lag} = 0.015$. Experimental data taken from [15].

can lead or lag due to ability of the yarns and coating to locally stretch. An inertial lag term,

$$\sigma_{lag}A = -C_{lag}m|\ddot{x}| = -C_{lag}mL|\ddot{\epsilon}| \quad (5)$$

where C_{lag} is a constant, A is the element area, m is the mass, and L is a length-scale of the problem, can model this effect. This term is added as a forcing function in LS-DYNA using the user-defined material mechanism. Figure 8 presents the computed uniaxial load cycles against the experimental data using the same bilinear elastic modulus as previously, along with the inertial lag term. The inertial lag does a reasonable job reproducing the hysteresis. As the proposed physics mechanism responsible for the hysteresis, and the lag model itself, both scale with sample size, this hysteresis and wander effect should be present at flight scale.

3.4 Lateral Contraction

During axial loading, lateral contraction of the fabric is observed, similar to the Poisson effect from solid mechanics. The ratio of the lateral to axial strain, ν_{12} in Eqn. 1, is plotted for the same two coated Kevlar fabrics in Fig. 9. The observed value of Poisson's ratio from these tests exceeds unity, which is inconsistent with standard isotropic and orthotropic models. In practice, Poisson's ratio is limited to values significantly lower than unity in orthotropic models to maintain numerical stability. For example, LS-DYNA enforces $\nu_{12} \leq 0.6$ in the MAT_FABRIC material model. The fabric lateral contraction is caused by the crimp interchange at low stress levels causing the lateral yarns to contract. Sebring and Freeston[17] model this behavior and predict lateral strain 1.8–5.4 greater than the axial strain, depending on the weave type, under uniaxial stress. The data in Fig. 9

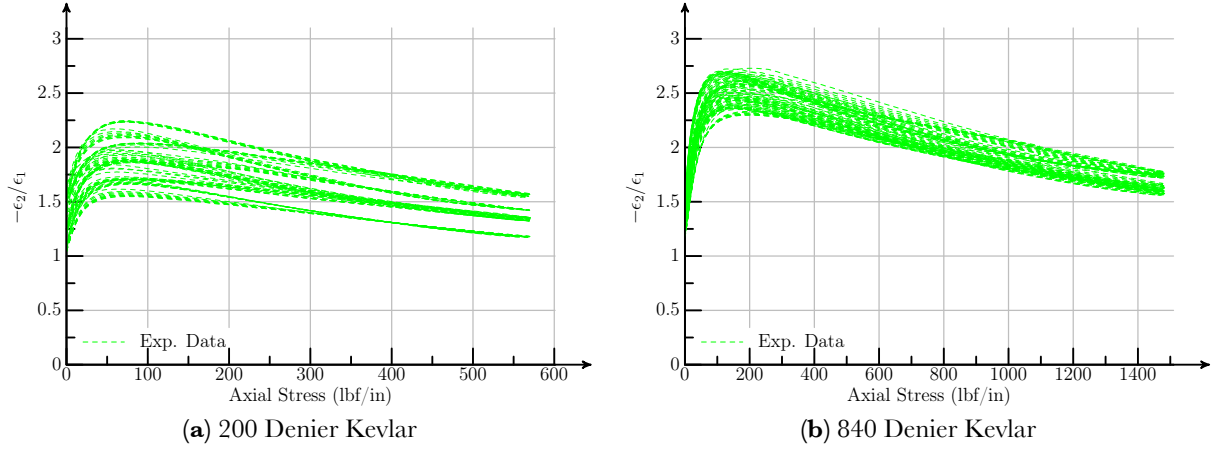


Figure 9: Ratio of lateral-axial strain during uniaxial loading for two silicone-coated Kevlar fabrics. Experimental data taken from [15].

is consistent with this model.

Separating the lateral and axial strain and replotting the data from Fig. 9 in Fig. 10 shows that the lateral contraction is solely due to the crimp interchange. After the initial contraction the lateral strain is essentially constant, with changes in ν_{12} being solely due to the continued increase in axial strain. This is due to the Poisson effect at high loading being confined to the individual fibres and yarns of the fabric, which is negligible relative to the width of the specimen. As with the elastic modulus, a bilinear approach separating the crimp interchange region from the remainder is used to test the modeling approaches, *i.e.*

$$\nu_{12} = \begin{cases} \frac{3}{4}\beta(\sigma_1, \sigma_2) & \text{if } \epsilon_1 \leq \epsilon^c, \\ 0 & \text{if } \epsilon_1 > \epsilon^c. \end{cases} \quad (6)$$

Figure 11 presents the computed bilinear model for lateral contraction against the experimental data. As expected, the simulated results do not produce the substantial lateral contraction seen in the uniaxial physical testing. Values of ν_{12} and ν_{21} greater than unity are inconsistent with an orthotropic model, and the complete lateral contraction response under uniaxial loading cannot be replicated using a homogenous FEM approximation. As noted in Sec. 3.1, for conditions of pure biaxial loading the crimp interchange region can be neglected and $\nu_{12} = \nu_{21} \approx 0$.

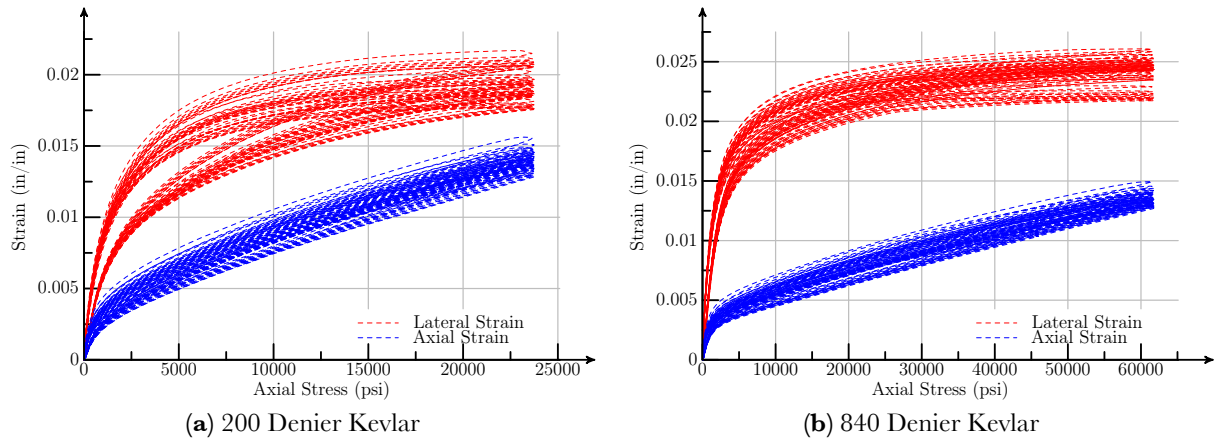


Figure 10: Variation of lateral and axial strain during uniaxial loading for two silicone-coated Kevlar fabrics. Experimental data taken from [15].

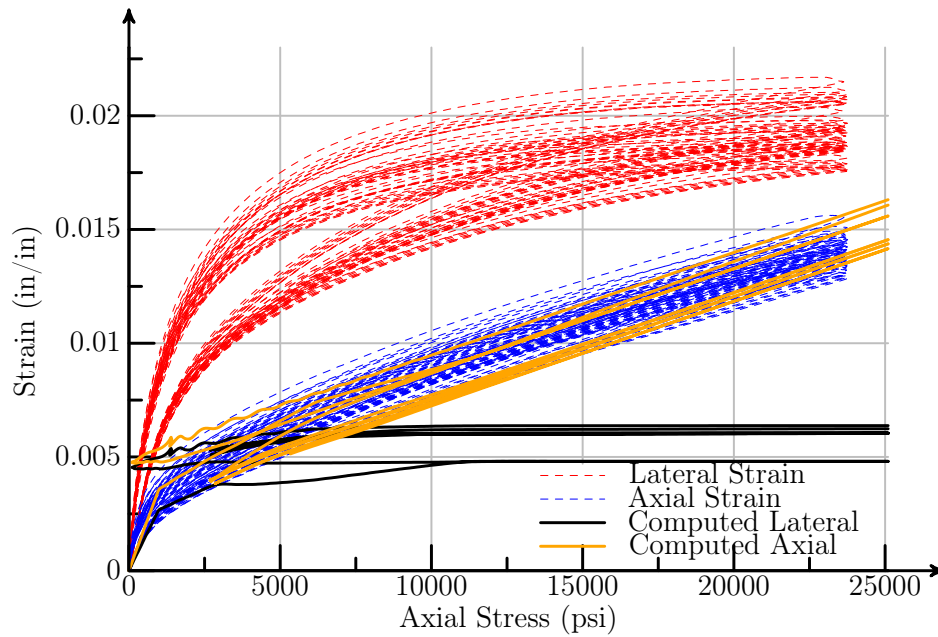


Figure 11: Variation of lateral and axial strain during uniaxial loading for two silicone-coated Kevlar fabrics. Experimental data taken from [15].

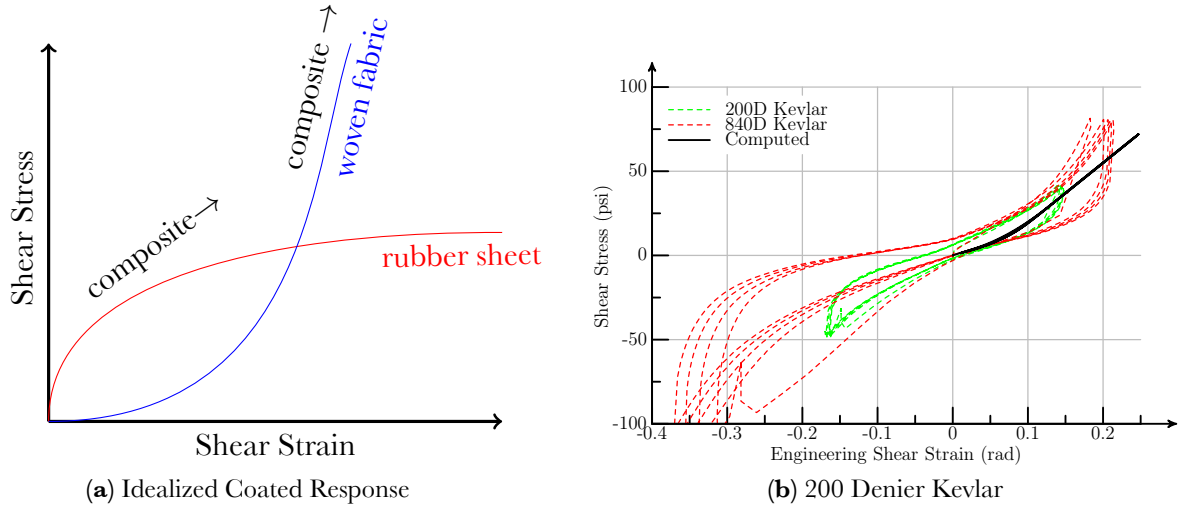


Figure 12: Shear stress-strain data for coated woven fabrics. Experimental data taken from [15].

3.5 Shear

The idealized shear stress-strain behavior of a coated woven fabric is presented in Fig. 12a (cf. [9]). A rubber sheet demonstrates a plastic response, while woven fabrics typically have a hyper-elastic response. The response of a coated woven fabric is typically a composite of these patterns, with the rubberized sheet dominating at low strain, and the woven fabric at higher strain. Figure 12b presents the shear stress-strain response from an 8 in. trellis-frame test apparatus for two coated Kevlar fabrics. Both fabrics demonstrate the expected behavior, with the initial response dominated by the silicone coating, and the higher-strain representative of the woven Kevlar. The shear modulus G_{12} for the initial loading regime for all silicone-coated samples tested in [15] is roughly 70 psi, which is in the expected range for a silicone rubber sheet. The shear modulus for the woven fabric region is estimated at $G_{12} = 360$ psi for the 200 denier Kevlar fabric. A simulation of the 200 denier Kevlar trellis-frame test using a bilinear shear model in LS-DYNA is included in Fig. 12b. The model agrees well with the observed behavior.* Note that the same hysteresis behavior due to stress relaxation discussed above for uniaxial loading is observed here for the shear response.

The shear stiffness increases with tension in the fabric. This is demonstrated using data from a pressurized cylindrical torsion rig which produces a biaxial loading. One end of an inflated fabric cylinder is torqued, while the opposite end is allowed to translate along the axis of rotation (cf. Hutchings *et al.* [14] for a full description). Data is obtained at two cylinder pressures (p_c), and the increase in shear modulus (slope) with increasing pressure is apparent (cf. Fig. 13a). Similar be-

*Only half the experimental loading cycle is simulated.

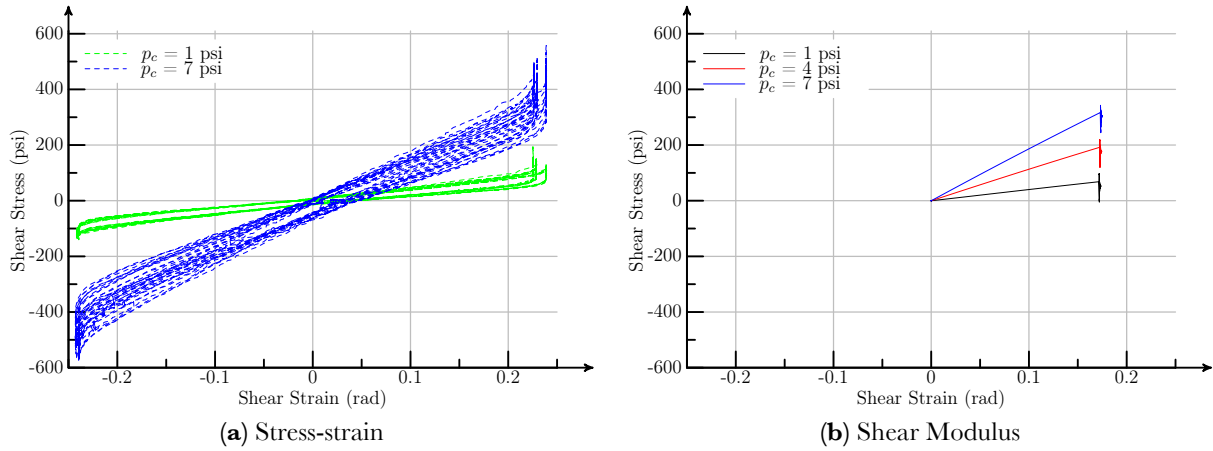


Figure 13: Shear strain variation during biaxial cylinder testing for silicone-coated 200 denier Kevlar fabric. Cylinder inflation pressures of $p_c = 1$ psi and 7 psi are reported. Experimental data taken from [15].

havior is seen in [14] for a urethane coated Kevlar fabric. Note that the shear stress-strain response under tension does not display the two-phase (rubber sheet - wove fabric) response seen in the trellis-frame test. In the trellis frame the fabric is initially under essentially zero tension load. It appears that inflating the cylindrical fabric sheet increases the distance between the yarns, thereby reducing the inter-yarn shear interactions, and providing a purely rubber sheet stress-strain response throughout the loading cycle. Simulations of the pressurized cylindrical fabric test support this conclusion. The increase in stiffness with loading is commonly handled by the geometric stiffness matrix in FEM. Using the fully-integrated shell element formulation and the `MAT_NONLINEAR_ORTHOTROPIC` material model in LS-DYNA provides this capability. The shear stiffness is held fixed at $G_{12} = 70$ psi, the observed value for the silicone rubber sheet portion of the trellis frame response, during simulations at increasing inflation pressure. The simulation results are presented in Fig. 13b, and display similar changes in stiffness with increasing tension as the experimental observations.

The scaling of the shear stiffness with increasing tension is essentially linear (cf. Fig. 14). In this configuration, with one set of fibers parallel to the irrotational axis of the shearing deformation, linear analysis[20] predicts $G_{12} = \sigma_1$. Both the experimental and computational data are consistent with this observation.

4 Summary

Simulating coated woven fabrics for IAD bladders with a homogenous assumption and a planar orthotropic material model has been investigated. A thin-shell FEM appropriate for predicting

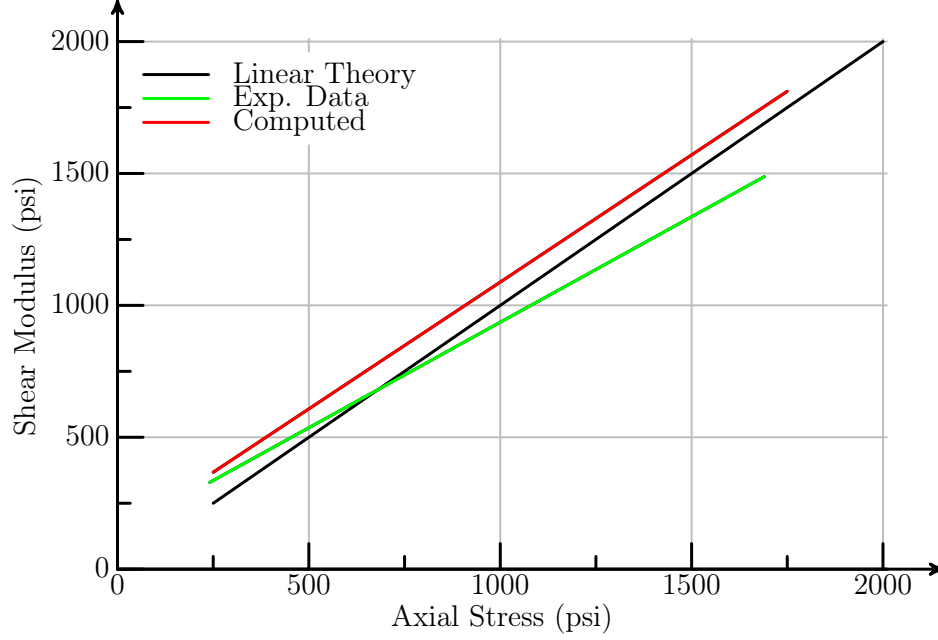


Figure 14: Variation of shear stiffness with increasing tension for pressurized cylinder test rig. Experimental data taken from [15].

the buckled response, and including higher-order geometric stiffening is recommended. Replicating experimental observations under general conditions relies on empirical modeling of the crimp interchange region. Several features of the fabric response, such as the lateral contraction under uniaxial loading and the stress/strain relaxation during load cycles, are difficult to replicate using standard FEM and a homogeneous assumption.

When appropriate to assume a strongly biaxial load, the desired engineering material model for inflatable decelerators reduces to a linear orthotropic model,

$$\begin{Bmatrix} \sigma_1 \\ \sigma_2 \\ \tau_{12} \end{Bmatrix} = \begin{bmatrix} E_1 & 0 & 0 \\ 0 & E_2 & 0 \\ 0 & 0 & G_{12} \end{bmatrix} \begin{Bmatrix} \epsilon_1 \\ \epsilon_2 \\ \gamma_{12} \end{Bmatrix} \quad (7)$$

with $G_{12} \approx 50 - 100$ psi, as appropriate for a rubber sheet. When necessary, the elastic moduli E_1 and E_2 can be estimated using fibre MDS data and the geometry of the fabric. It is important to note that while Eqn. 7 contains many simplifications, it is by understanding the fabric behavior that we are able to interpret the experimental observations and tailor the model for the high-tension environment of inflatable decelerators.

There are several outstanding issues from the current work. The first is the observed hysteresis,

and developing a suitable method for modeling the behavior. Currently only sub-scale test data and a tentative hypothesis for the cause of the hysteresis are available. Understanding how the stress-strain relaxation scales with increasing size, and the timescales of the relaxation are important. This information must be obtained by suitable physical testing. The uncertainty in the observed stress in Fig. 3 is $\pm 30\%$ from the median at 0.01% strain. Another outstanding issue is the transition of shear behavior from rubber sheet to woven fabric when the structure is under tension. It is unclear if this transition does occur, and under what conditions, if the shear loading is increased beyond that observed in the pressurized cylinder test apparatus. Lastly, to develop a general biaxial model, either empirical or predictive, appropriate biaxial test data must be obtained for coated woven fabrics.

Acknowledgments

The authors would like to thank the staff at ILC Dover for their support of this project through procurement of the coated fabrics samples and providing the material test data. Doug Sanders of ASRC Research and Tech Solutions provided invaluable assistance in using LS-DYNA. Prof. Peter Gosling and Dr. Ben Bridgens, of Newcastle University, UK generously allowed reproduction of their fabric micrographs.

References

- [1] Braun, R.D. and Manning, R.M., “Mars Exploration Entry and Landing Challenges,” *Journal of Spacecraft and Rockets*, 44(2):310–323, March 2007.
- [2] Christian, J., Wells, G., Lafleur, J., Verges, A., and Braun, R., “Extension of Traditional Entry Descent and Landing Technologies for Human Mars Exploration,” *Journal of Spacecraft and Rockets*, 45(1), January 2008.
- [3] Huang, Z.M. and Ramakrishna, S., “Micromechanical Modeling Approach for the Stiffness and Strength of Knitted Fabric Composites: A Review and Comparative Study,” *Composites: Part A*, 31(5):479–501, 2000.
- [4] Tabiei, A. and Ivanov, I., “Computational Micro-mechanical Model of Flexible Woven Fabric for Finite Element Impact Simulation,” *International Journal for Numerical Methods in Engineering*, 53(6):1259–1276, 2002.
- [5] Boisse, P., Zouari, B., and Daniel, J-L., “Importance of in-plane shear rigidity in finite element analyses of woven fabric composite preforming,” *Composites: Part A*, 37:2201–2212, 2006.

- [6] Lin, H., Clifford, M.J., Long, A.C., and Sherburn, M., “Finite element modelling of fabric shear,” *Modelling and Simulation in Materials Science and Engineering*, 17:1–16, 2009.
- [7] Leaf, G.A.V., “Analytical Plain Weave Fabric Mechanics and the Estimation of Initial Shear Modulus,” *Journal of the Textile Institute*, 92(3):70–79, 2001.
- [8] Cavallaro, P.V., Sadegh, A.M., Quigley, C.J., and Johnson, A.R., “Effects of Coupled Biaxial Tension and Shear Stresses on Decrimping Behavior in Pressurized Woven Fabrics,” NUWC-NPT Technical Report 11,571, October 2004.
- [9] Farboodmanesh, S., Chen, J., Mead, J., and White, K., “Effect of Fabric Construction on Mechanical Behavior of Rubber Reinforced Fabric,” *Rubber Chemistry and Technology*, 79(2): 119–216, 2006.
- [10] Potluri, P., Perez Ciurezu, D. A., and Young, R.J., “Biaxial Shear Testing of Textile Preforms for Formability Analysis,” in *16th International Conference on Composite Materials*, 2007.
- [11] Gosling, P.D. and Bridgens, B.N., “Material Testing and Computational Mechanics - A New Philosophy for Architectural Fabrics,” *International Journal of Space Structures*, 23(4):215–232, 2008.
- [12] King, M.J., Jearanaisilawong, P., and Socrate, S., “A Continuum Constitutive Model for the Mechanical Behavior of Woven Fabrics,” *International Journal of Solids and Structures*, 42: 3867–3896, 2005.
- [13] Hirokazu, M., “A Multi-Step Linear Approximation Method for Nonlinear Analysis of Stress and Deformation of Coated Plain-Weave Fabric,” *Journal of Textile Engineering*, 52(5):189–195, 2006.
- [14] Hutchings, A.L., Braun, R.D, Masuyama, K., and Welch, J.V., “Experimental Determination of Material Properties for Inflatable Aeroshell Structures,” AIAA Paper 2009-2949, 2009.
- [15] Lin, J.K., Shook, L.S., Ware, J. S., and Welch, J.V., “Flexible Material Systems Testing,” NASA Contractor Report CR-2010-AC89D, May 2010.
- [16] Tanner, C.L., Cruz, J.R., Hughes, M.F, Clark, I.G., and Braun, R.D., “Subsonic and Transonic Wind Tunnel Testing of Two Inflatable Aerodynamic Decelerators,” in *Proceedings of the 7th International Planetary Probe Workshop*, June 2010.

- [17] Sebring, R.E. and Freeston, Jr., W.D., “Biaxial Tensile Tester for Fabrics,” Fabric Research Laboratories, Technical Report, May 1967.
- [18] Freeston, Jr., W.D., Platt, M.M., and Schoppee, M.M., “Mechanics of Elastic Performance of Textile Materials, Part XVIII, Stress-Strain Reponse of Fabrics Under Two-Dimensional Loading,” *Textile Research Journal*, 37:948–975, 1967.
- [19] Hearle, J.W.S. and Shanahan, W.J., “An Energy Method for Calculations in Fabric Mechanics, Part I: Principles of the Method,” *Journal of the Textile Institute*, 69:81–91, 1978.
- [20] Topping, A., “An Introduction to Biaxial Stress Problems in Fabric Structures,” *Aerospace Engineering*, 20:18–19, 53–58, 1961.
- [21] Kramer, R., Cirak, F., and Pantano, C., “Fluid-structure Interaction Simulation of an Inflatable Aerodynamic Tension-cone Decelerator,” AIAA Paper 2010-4608, July 2010.